A pin-on-disc study on the dry sliding behavior of a Cu-free friction material containing different types of natural graphite

Mara Leonardi, Mattia Alemani, Giovanni Straffelini, Stefano Gialanella

PII: S0043-1648(19)31338-9

DOI: https://doi.org/10.1016/j.wear.2019.203157

Reference: WEA 203157

To appear in: *Wear*

Received Date: 4 September 2019

Revised Date: 8 November 2019

Accepted Date: 10 December 2019

Please cite this article as: M. Leonardi, M. Alemani, G. Straffelini, S. Gialanella, A pin-on-disc study on the dry sliding behavior of a Cu-free friction material containing different types of natural graphite, *Wear* (2020), doi: https://doi.org/10.1016/j.wear.2019.203157.

A pin-on-disc study on the dry sliding behavior of a Cu-free friction material containing different types of natural graphite

Mara Leonardi[a], Mattia Alemani[b], Giovanni Straffelini[a], Stefano Gialanella[a]

[a] Dept. of Industrial Engineering, University of Trento, Via Sommarive 9, Povo, Trento, Italy
[b] Brembo S.p.A., Stezzano, Bergamo, Italy

KEYWORDS

Natural graphite; brake materials; pin-on-disc tests; friction layer.

ABSTRACT

This research investigates the influence of graphite's granulometry on the dry sliding behavior of a copper-free friction material against pearlitic cast iron.

Samples were designed and fabricated using three different types of commercial natural graphite. A sample without graphite was also considered as a reference. Tests were carried out with a pin-on-disc tribometer at room temperature (RT), at 400°C, and at RT after the high temperature tests.

The results show that both the shape and size of the graphite particles influence the coefficient of friction and the specific wear rate. The friction material featuring a lower particle size and equiaxed grains of natural graphite exhibits a better behavior, as compared to coarser graphite with plate-like grains. The results were obtained comparing specific characteristics (i.e., morphology and chemical composition) of the friction layers formed on each friction material under the different testing conditions.

1.INTRODUCTION

An important research topic regarding brake pads for passenger cars is related to recent regulations aiming at reducing the use of copper. Indeed, the U.S. legislation currently requires copper to be reduced down to 0.5% by 2025 [1]. Nevertheless, copper has important properties, such as high thermal conductivity and the ability to stabilize the friction coefficient, that are beneficial to the brake pad performances [2][3]. Therefore, in view of the ban of copper, potential alternatives able to counterbalance its replacement need to be investigated.

Organic friction materials used to produce automotive brake pads are made of several constituents [4]. The friction material components, often more than 20, are classified according to their main role as: reinforcements, binders, fillers and friction additives [5][6]. The friction additives can be classified into two further types: lubricant and abrasive. Lubricants are friction coefficient stabilizer and help regulating the generation of the friction layer, therefore contributing to wear reduction. A smooth sliding behavior, i.e. the stabilization of the friction coefficient, is essential for good brake performances. In these regards, various metal sulfides and graphite are commonly used in the brake pad formulations [7].

Among these, graphite is regarded as one of the strategic constituents in the development of copper-free formulations for different reasons [8]. First, its high thermal conductivity, between 350 and 250 $WK^{-1}m^{-1}$, i.e., is close to the thermal conductivity of copper, although, copper is far less sensitive to temperature than graphite [9]. Moreover, studies on the contact area performed by Österle et al. [10], suggest that soft inclusions, like graphite in the friction layer, as well as copper, result in the stabilization of the friction coefficient, and induce a smoother sliding behavior.

Several studies on graphite are reported in the literature for copper-based friction materials [11][12][13], in which graphite is one of the most important components. Different types of graphite are used as ingredients, either synthetic or natural, and with different grain morphologies [14]. Graphite is also widely studied in organic friction materials, mainly in those that also contain copper.

In general, it can be stated that not every form of graphite is suitable to improve the friction material performances [15]. Synthetic graphite has been broadly studied, considering different aspects, including its influence on the sensitivity of friction coefficient and wear rate to braking pressure and sliding speed [16], and its noise emission contribution [17]. The studies, however, suggest more than a range of synthetic graphite particle size, both coarse and fine. Also thermal conductivity has been extensively investigated, as concerns especially treated graphite [18][19], to reach a satisfactory value. Concerning natural graphite, a few studies on its properties as a component in friction materials can be found in the literature, mostly in comparison with a synthetic counterpart. D.K. Kolluri et al. [20] studied the effect of fine particle granulometries on the thermal localization phenomenon in a

composition involving also brass, finding that the particle size is the main parameter which influences the friction coefficient. However, wear rate was not taken into consideration for these materials.

Although graphite is regarded as a possible replacement for copper, a few research studies only have been dedicated to study graphite in Cu-free formulations, and just a few of them investigated the influence of graphite on the relevant tribological properties (friction and wear) at different testing temperatures.

The present research used a pin-on-disc tribometer to correlate specific test conditions, including the temperature of the disc, to fundamental tribological mechanisms in Cu-free base formulations, each one of them prepared by adding to a reference masterbatch a given concentration of different types of natural graphite, featuring different particle size and morphology. The tribological performances of the novel formulations were comparatively investigated on a pin-on-disc (PoD) tribometer. Notoriously, this set up cannot replicate real brake system action, for which specific types of experimental equipment, e.g., dyno-bench tests, are available. However, PoD can comparatively investigate in a timely manner the influence that specific composition and test conditions have on the material performances. Tests were performed at room temperature (RT) and 400°C. Concerning RT, the tests were conducted also on the sample already tested at 400°C. This was meant to investigate the recovery capability of the diverse friction materials. Microscopy observations and elemental analyses were conducted on the friction layer that builds upon the worn pin's surface, to obtain a solid interpretation of the tribological results.

2. MATERIALS AND METHODS

2.1 MATERIALS

A masterbatch of a low-metallic friction material not containing graphite was used as a reference for this study. The composition of the material, measured by energy dispersive X-ray spectroscopy (EDXS), is shown in **Table 1**. The main components can be classified according to standard categories as: reinforcing fibers (steel fibers); friction additives (aluminum oxide, tin sulfide, magnesium oxide, zinc oxide, coke); fillers (vermiculite, calcium carbonate)**;** binder (phenolic resin). **Fig. 1** shows an SEM micrograph, in which some of main constituents of the reference friction material are labelled.

Table 1. Elemental composition of the masterbatch used as reference. Carbon not quantified.

Element	**Fe**	**O**	**Zn**	**Mg**	**Al**	**S**	**Sn**	**Ca**	**Si**	**Cr**
wt%	26.0	36.2	1.4	12.2	8.1	3.9	6.6	1.2	1.4	3.0

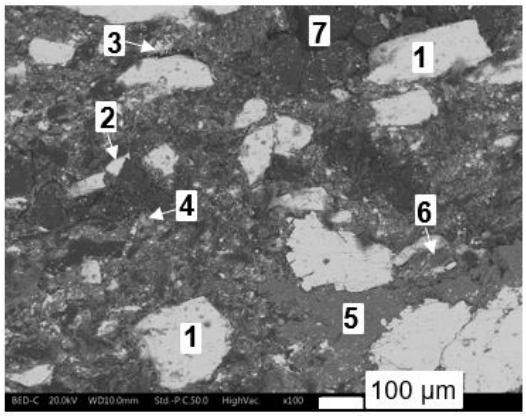

1. Iron fibers
2. Zinc
3. Tin Sulfide
4. Chromite
5. Vermiculite
6. Magnesium oxide
7. Coke

Fig.1 SEM micrograph of the reference masterbatch with indication of some of the main constituents.

Three different types of natural graphite, featuring a diverse particle size, were selected. In **Fig. 2** the scanning electron microscopy (SEM) micrographs with the morphology of these three types of graphite are shown. The graphite # 1 is a flake graphite with the particle size in the 300 – 425 µm range. The graphite # 2 has a flake morphology, with the grain size below 100 µm. The graphite # 3 is a fine granular graphite with particle size below 40 µm. The main features of the selected graphite are summarized in Table 2.

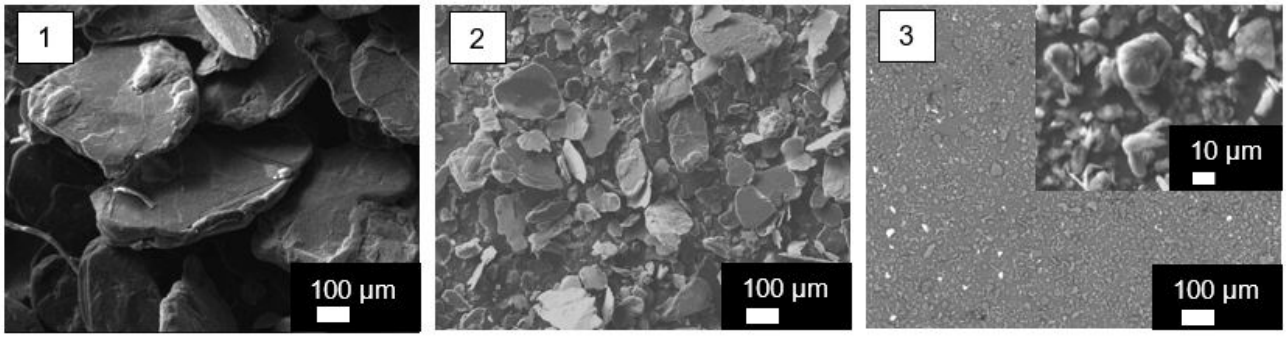

Fig. 2 SEM micrographs of the natural graphite (1, 2, 3) with different particle size.

Table 2. Specifications of the three types of natural graphite (1, 2, 3). d_{90} indicates that 90% of the sample is above/below the specified value.

	Supplier	**Content of C**	**Graphite grade**	**Particle size, d_{90} (µm)**
1	Imerys	94-97%	Flake	> 300
2	AMG	94-96%	Small flake	< 100
3	AMG	96-98%	Very fine grinding	< 40

The powder mixtures were prepared by adding 9 wt% of graphite to the reference masterbatch, mixer-milled for 20 minutes using a Turbula shaker-mixer. The concentration of graphite is representative of concentrations used in other studies on friction material, with a particular focus on graphite [21][17]. In **Table 3** the formulations of the prepared mixes and their designations are displayed. The materials were codenamed *Ref.* (the reference masterbatch without graphite), *N1* (the mixture with the addition of natural flake graphite #1), *N2* (the mixture with the addition of natural flake graphite #2) and *N3* (the mixture with the addition of natural granular graphite #3).

Table 3. Composition (wt%) and designation of the friction material samples.

Designation	Masterbatch	Graphite 1	Graphite 2	Graphite 3
Ref.	100 wt%	-	-	-
N1	91 wt%	9 wt%	-	-
N2	91 wt%	-	9 wt%	-
N3	91 wt%	-	-	9 wt%

Each tribological test specimen was prepared by pressing roughly 2 g of powder mix in a mold of a hot-pressing apparatus with a pressure of 17 MPa. In this way, cylindrical pins with a diameter of 10 mm and a height of 10 mm were obtained. The samples were cured for 15 min at 150°C, and successively post-cured in an oven for 7h at 200°C in air.

The density of the pins, evaluated as the mass of each pin divided by its volume, was 2.29 ± 0.06 g/cm^3 for the *Ref.* and 2.18 ± 0.04 g/cm^3 for the pins with graphite (*N1*, *N2*, *N3*).

Discs made of pearlitic grey cast iron with a diameter of 60 mm and 6 mm in height, with the hardness of 235 HV10 were used as counterface for the tribological tests.

2.2 EXPERIMENTAL PROCEDURE

The friction and wear properties of the samples were firstly characterized running room temperature (RT) PoD tests. The tribometer used for the tests, equipped with a heating system for the disc, was manufactured by Ducom Instruments.

The sliding velocity was 1.5 m/s and the nominal contact pressure was 1 MPa in all cases. These conditions, used in previous investigations, are intended to obtain mild wear sliding conditions [22][23]. The duration of each test was 90 min. and before each test a 30 min. run-in period was performed. Four tests were conducted for each sample at room temperature.

High temperature tests at 400°C (*HT*) were carried out using an induction heating apparatus to heat up the disc. A closed loop feedback control system kept the temperature constant throughout the test, using an infrared high temperature sensor. It is important to note that the HT tests were started after

the disc temperature reached 400°C. During the heating-up of the disc the pin was lifted, and repositioned only once everything was ready to start the test, including a stable temperature. The duration of these tests was 60 min. only, instead of 90 min., because of the more demanding conditions.

The *HT* tests were then followed by further room temperature tests, still on the same specimens: *RT_after HT* test. Two test runs were conducted for the evaluation of the specific wear rate. For this purpose, each pin had to be removed from the testing equipment when passing from the *HT* to the *RT_after HT* test, since its weight had to be measured at the beginning and at the end of each test. Two more tests were conducted for a more reliable observation of the evolution of the friction coefficient. In this latter case, the pin was not removed from the test rig for the whole duration of the test sequence.

The friction coefficient was continuously recorded using a load cell. The wear rate was assessed by weighting the test sample before and after each run with an analytical balance having a 10^{-4} g sensitivity. The wear of the pin was estimated using the specific wear coefficient (K_a), given by:

$$K_a = V / F_n\, s \qquad Eq.(1)$$

where V [m^3] is the measured wear volume, calculated using the bulk density; F_n [N] is the applied load; s [m] is the sliding distance.

The worn surface of the pins was observed with a JEOL IT300 scanning electron microscope, equipped with an EDXS system. The pins were observed both in section and planar view. Cross sections have been prepared by cutting the samples, embedded in epoxy resin, along longitudinal to the sliding direction, in order to evaluate the thickness and the compactness of the friction layer. The planar view of the pin surface, carried out prior to mounting the samples in resin for the cross-sectional observations, were mainly focussed on measuring the extension of the friction layer and to evaluate the composition of the primary and secondary plateaus.

3.RESULTS

3.1 FRICTION AND WEAR BEHAVIOUR

Fig. 3 shows the evolution of the friction coefficient (μ) during the PoD tests at room temperature (RT). After an initial run-in stage with a duration of approximately 2500 s, all samples reached a steady-state, whose relevant mean friction coefficients are listed in **Table 4**. The two samples having smaller graphite grains, namely *N2* and *N3*, show an evident decrease in μ with respect to the reference material (*Ref.*), having a coefficient of friction similar to that of the *N1* material.

The experimental specific wear coefficients (K_a) are also summarized in **Table 4** and displayed for a better comparison in **Fig. 4**. The *Ref.* and *N1* materials show higher K_a values than N2 and N3, and also larger scatters, as evidenced by the standard deviation bars. Material *N3* displays the lowest wear rate and steady-state friction coefficient.

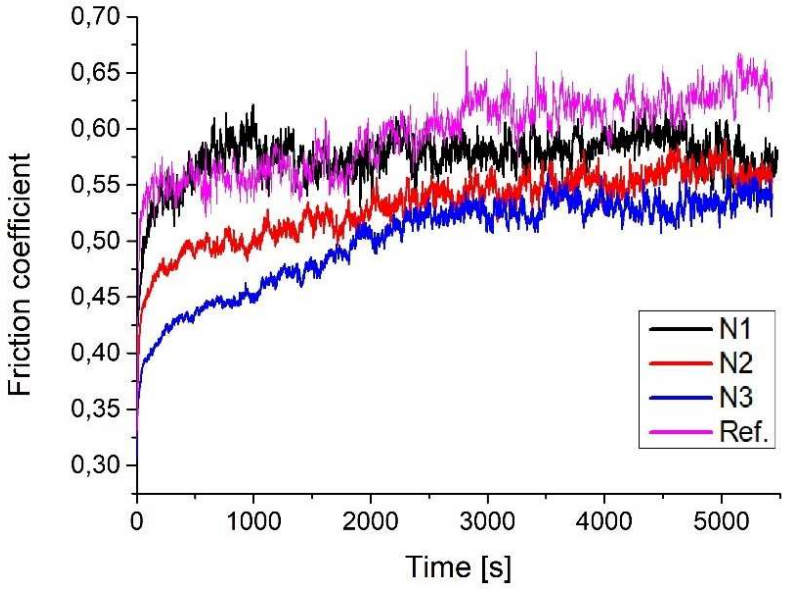

Fig. 3 Coefficient of friction recorded during the pin-on-disc tests at RT. Samples: Ref. and materials with the addition of natural graphite N1, N2 and N3.

Table 4. Pin-on-disc tests at RT: values of friction coefficient calculated in the steady-state (μ_{ss}) and the specific wear coefficient (K_a).

Sample	**μ_{ss}**	**K_a** [m^2/N]
Rif.	0.62 ± 0.02	(7.2 ± 0.8) *10^{-14}
N1	0.58 ± 0.01	(5.7 ± 1.2) *10^{-14}
N2	0.56 ± 0.01	(4.8 ± 0.3) *10^{-14}
N3	0.52 ± 0.02	(4.2 ± 0.2) *10^{-14}

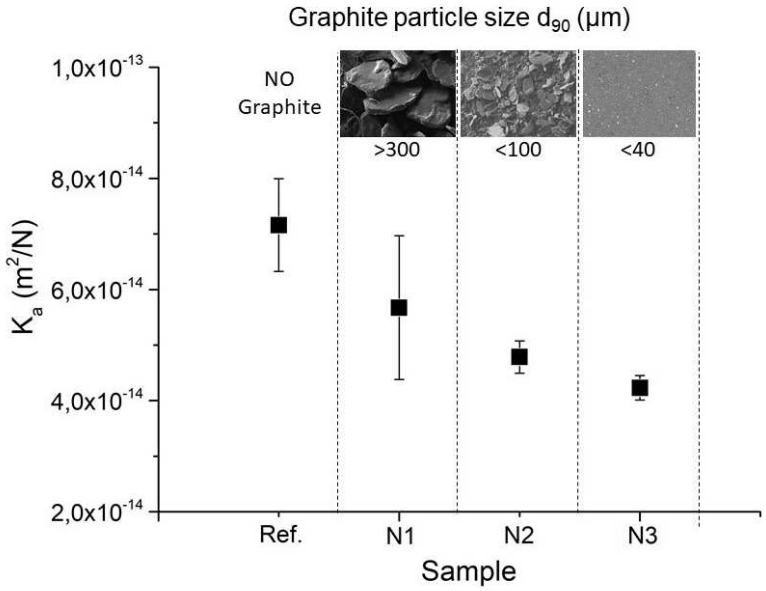

Fig. 4 Mean values of the specific wear coefficient (K_a) calculated for the pin-on-disc tests at RT. Samples *Ref. (NO Graphite)*, *N1*, *N2*, and *N3*.

The evolution of the friction coefficient of the *Ref.* sample at 400°C and during the subsequent *RT_after HT* test is displayed in the graphs in **Fig. 5**. The friction coefficient curve exhibits different stages. At the beginning, it increases up to a peak value and then decreases. Successively, it starts increasing again up to a second peak, and then progressively decreases down to the steady-state value (the obtainment of a steady-state after approximately 3000 s of sliding was observed also during longer tests, not reported herewith). This particular behaviour was observed in all the friction materials prepared for the present study.

After cooling the disc down to RT, the PoD test was restarted to check how the *HT* test had influenced the friction and wear behaviour of these materials (**Fig. 5b**). In this case, quite a long run-in stage was observed, with a continuous raise in the friction coefficient, again followed by steady-state conditions which were reached close to the end of the test. The experimental values of the friction coefficient once the steady-state was achieved, are indicated in **Table 5**.

These combined tribological tests, involving a high temperature followed by a room temperature run, resulted particularly useful to evaluate variations in the µ value induced by the high temperature conditions, as compared to the values measured with the tests conducted at *RT*. To calculate the percent variation of the steady-state friction coefficient, between the values obtained at *HT* and the RT values (*RT*), and between these values obtained, still at *RT, but* after the test at *HT* (*RT_after HT),* the following equations have been used:

$$\%\mu_{HT} = \left(\frac{\mu_{HT} - \mu_{RT}}{\mu_{RT}}\right) x\ 100 \qquad \textit{Eq. (2)}$$

$$\%\mu_{RT\_afterHT} = \left(\frac{\mu_{RT\_HT} - \mu_{RT}}{\mu_{RT}}\right) x\ 100 \qquad \textit{Eq. (3)}$$

The change of μ ($\%\mu_{HT}$ and $\%\mu_{RT\_afterHT}$) are also included in **Table 5**. The comparative graphs in **Fig. 6** show how the graphite influences these changes in the friction coefficients. All tested materials show a similar reduction in μ after the test at *HT*. The largest decrease, 22%, was found with the *N1* sample.

The situation is different for the RT tests carried out after the HT tests. The *Ref.* sample actually recovers its μ ($\%\mu_{RT\_afterHT}$= 2%), whereas all other samples exhibit an incomplete recovery of the friction coefficient. Among these samples, *N3* exhibits the best recovery ($\%\mu_{RT\_afterHT}$ = -8%), whereas the worst behavior is displayed by *N2* ($\%\mu_{RT\_afterHT}$ = -19%).

The specific wear coefficient calculated for all the tested pins is shown in **Fig. 7**. *Ref.* material exhibits an increase in wear rate passing from *RT* tests to *HT* tests and to the *RT* tests after *HT* tests. The materials with graphite also exhibit an increase in wear rate passing from *RT* tests to *HT* tests; whereas a reduction was observed in the *RT* tests conducted after *HT* tests. In general, materials containing graphite show lower values of K_a with respect to the *Ref.* material, except for material *N1* at *RT* and *HT*. The material *N3* has the best wear performance for all the tested conditions.

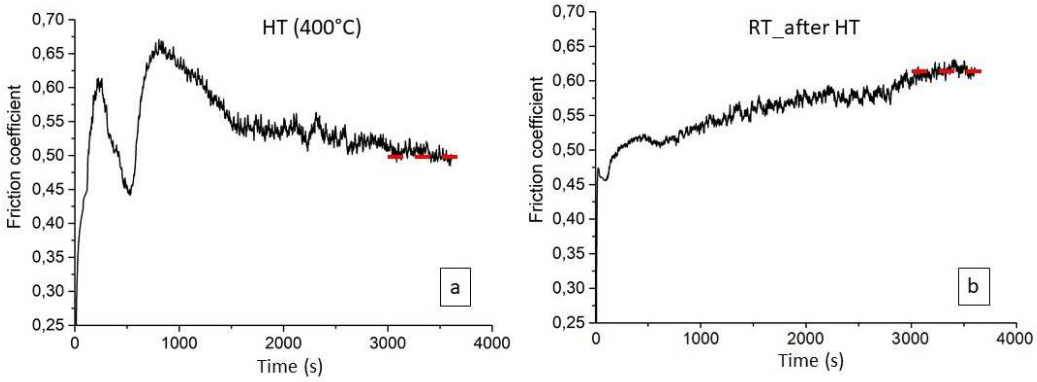

Fig. 5 Sample *Ref.* - Evolution of the friction coefficient with time during the tests at high temperature *(a)*, followed by the test at RT (b), *RT_after HT*.

Table 5. Friction coefficient values of pins Ref., N1, N2, N3 tested under the following different conditions: high temperature 400°C (HT) and RT after the test at HT (RT_after HT). The changes of friction calculated with the equations indicated in the main text are also reported ($\%\mu_{HT}$ and $\%\mu_{RT\_afterHT}$).

	$\mu_{steady\text{-}state}$		Variation of friction coefficient (%)	
Samples	**HT (400°C)**	**RT_after HT**	**$\%\mu_{HT}$**	**$\%\mu_{RT\_afterHT}$**
Ref.	0.51	0.63	- 18 %	+ 2 %
N1	0.45	0.51	- 22 %	- 12 %
N2	0.45	0.45	- 19 %	- 19 %
N3	0.43	0.48	- 17 %	- 8 %

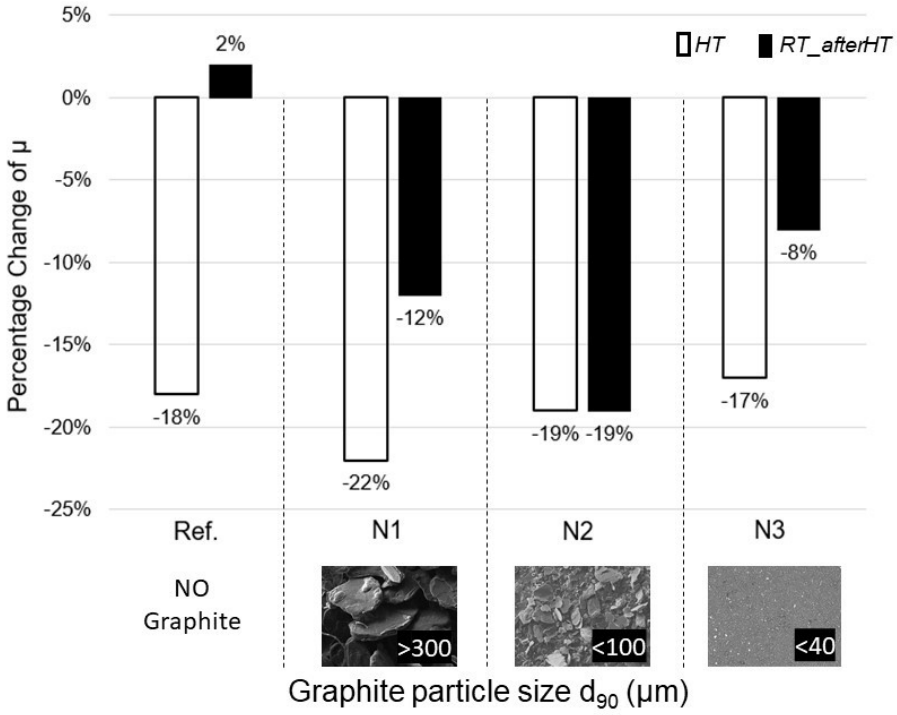

Fig. 6 Change in the friction coefficients, μ_{HT} (%) and $\mu_{RT\_afterHT}$ (%), as a function of the composition of the investigated materials.

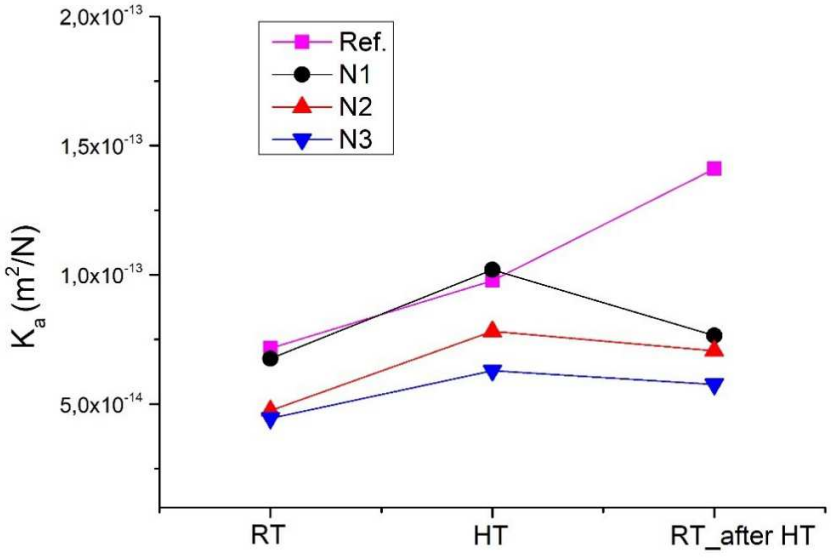

Fig. 7 Specific wear coefficient, K_a (m^2/N), calculated for the samples tested at room temperature (*RT*), high temperature (*HT*, 400°C) and RT after the test at HT (*RT_after HT*).

3.2 ANALYSIS OF WORN SURFACES

In **Fig. 8** the cross-section views for PoD samples tested at *RT* are displayed. The arrows help to identify the secondary plateaus on the pins surface, that result from the compaction of wear debris piling up at the primary plateaus, according to a very well established mechanism [6][22].

The secondary plateaus in the *Ref.* sample are made by coarse and weakly compacted particles.

The *N1* sample is similar to *Ref.* concerning the plateau's thickness (around 30 μm) and grain size of the wear particles, which look more compacted than in the *Ref.* sample. A different situation has been found on the surface of the *N2* and *N3* samples, both being characterized by the presence of quite dense and compacted secondary plateaus, well anchored to the pin surface.

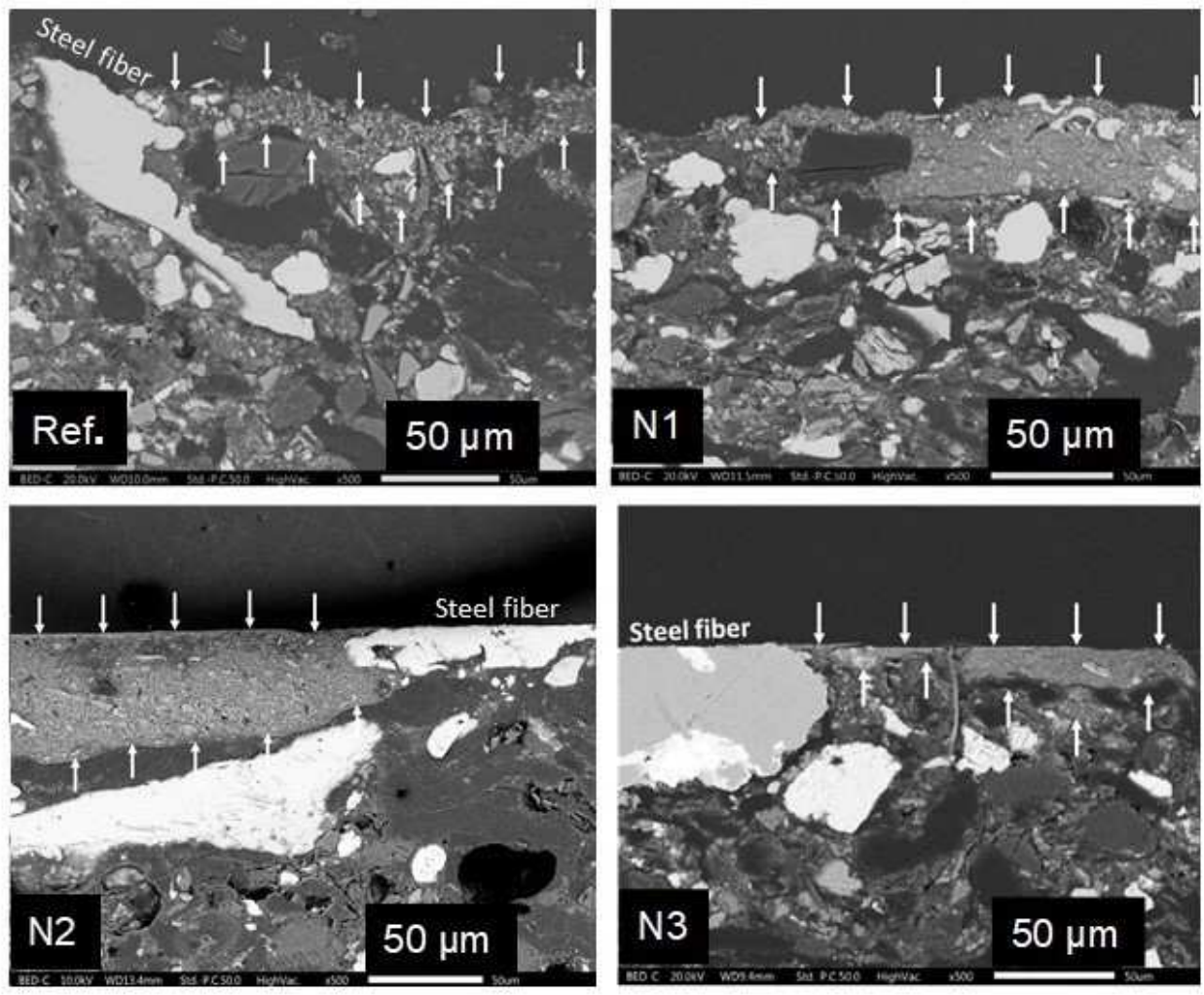

Fig. 8 Cross-section of the worn pins after the pin-on-disc tests at *RT*. The arrows indicate the secondary plateaus.

The planar views of the worn pins tested at *RT* are shown in **Fig. 9**. The *Ref.* sample features a large area covered with wear debris, but just small portions of its surface (II), near the primary plateaus (I), are well compacted.

This observation is coherent with the cross-section images in **Fig. 8**. On the *N1* sample surface, the secondary plateaus are definitely wider, but they are also characterised by several cracks. On the surface of *N2* sample, the plateaus are smaller and more regularly distributed even if some cracks are present in this case too. The secondary plateaus on the *N3* sample are even smaller but without fractures: this indicates good compaction of the constituents and better mechanical properties of the resulting plateaus (**Fig. 9**).

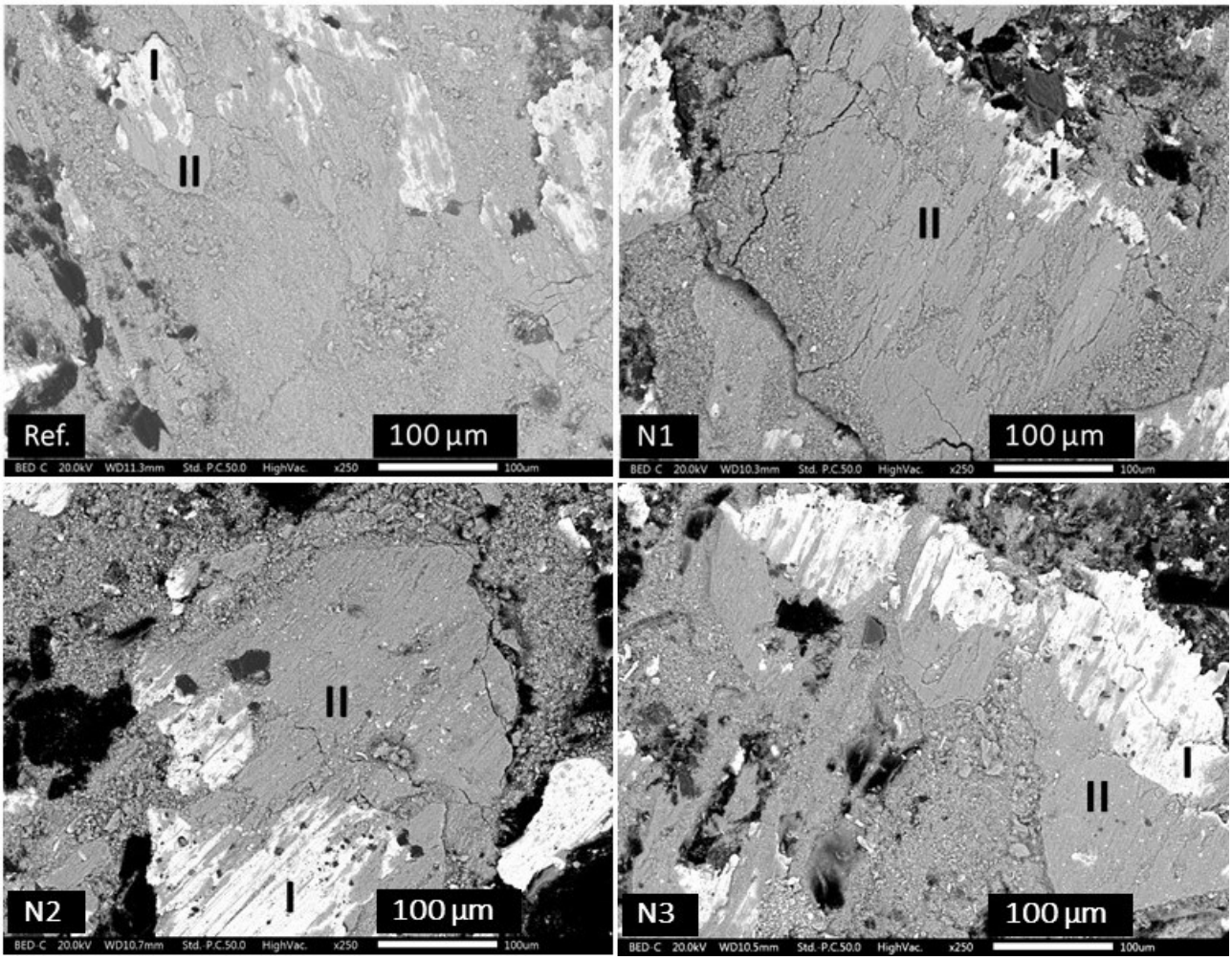

Fig. 9 Planar view of the worn pins after the pin-on-disc tests at *RT*. In the observations are visible for all the samples (*Ref.*, *N1*, *N2*, *N3*) the primary plateaus (I), mainly made by steel fibers, and the secondary plateaus (II).

In **Table 6** a summary of the main features of the secondary plateaus are given, as obtained from the SEM observations of the cross-section and planar views of the samples tested at *RT*, i.e. average thickness, compaction degree, extension and presence of cracks.

Table 6. Main features of the secondary plateaus of the samples *Ref.*, *N1*, *N2*, *N3 at RT*.

Material	Average thickness (μm)	Compaction degree	Extension	Presence of cracks
Ref.	30	low	low	no
N1	35	medium	large	yes
N2	40	good	medium	yes
N3	20	good	medium	no

Table 7 provides the compositional results of the EDXS analyses carried out on the secondary plateaus (regions II in **Fig. 9**). The majority element is iron, which comes both from the disc and pin. This element is present in the friction layer mainly in the form of mixed oxides [25][26][27]. The concentrations of the other elements in the secondary plateaus, coming mainly from the wearing out of the pin, are not so different from one sample to another. Particular attention was paid to the relative content of carbon in the plateaus of the different samples. The *Ref.* and *N1* samples have the same content, 7.0 wt%. Whereas the concentration of C increases in the plateaus of *N2* and *N3* samples, reaching the values of 8.2 wt% and 9.3 wt%, respectively.

Table 7. EDXS analyses on the secondary plateaus of the samples *Ref.*, *N1*, *N2*, *N3* tested at ***RT***. Concentrations in wt.%.

	Ref.	N1	N2	N3
Fe	61.2	62.0	58.5	55.2
O	18.1	17.7	19.4	20.1
C	7.0	7.0	8.2	9.3
Zn	3.4	3.3	3.7	3.4
Sn	2.0	2.0	2.1	2.0
Mg	2.0	1.6	1.8	2.2
Al	1.9	1.8	1.7	2.3
S	1.8	1.9	1.8	1.9
Si	1.3	1.3	1.3	2.1
Cr	0.7	0.8	0.8	0.8
Ca	0.6	0.6	0.7	0.7

In **Fig. 10,** the top view of the friction layer that formed on the surface of the *Ref.* material after the *HT* test is shown. This observation is representative of all the materials tested at 400°C, exhibiting a similar behavior. The friction layers are made of wear debris that are not compacted to form stable secondary plateaus, like those observed at RT (**Fig. 9**).

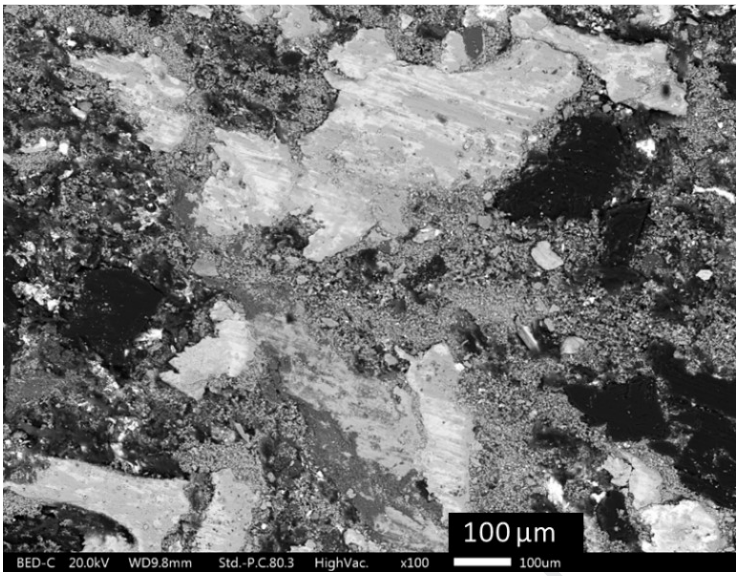

Fig. 10 Planar view of the *Ref.* material after the pin-on-disc tests carried out at 400°C (*HT condition).*

Fig. 11 shows SEM micrographs of the planar views of the friction layers present on the worn pins after the tests carried out in the *RT_after HT* condition. The materials with the addition of graphite (*N1*, *N2*, *N3*) display a similar surface morphology as those tested at *RT*. The pin surface still features regions with well-compacted layers of debris, together with other regions in which debris are not compacted. The secondary plateaus of the *Ref.* sample appear smaller than in the samples with graphite.

In **Table 8** the EDXS analyses carried out on the secondary plateaus of the samples tested at *RT_after HT* are summarized. Also, in this test condition, the main elements detected for all the samples are Fe, O, C and Zn.

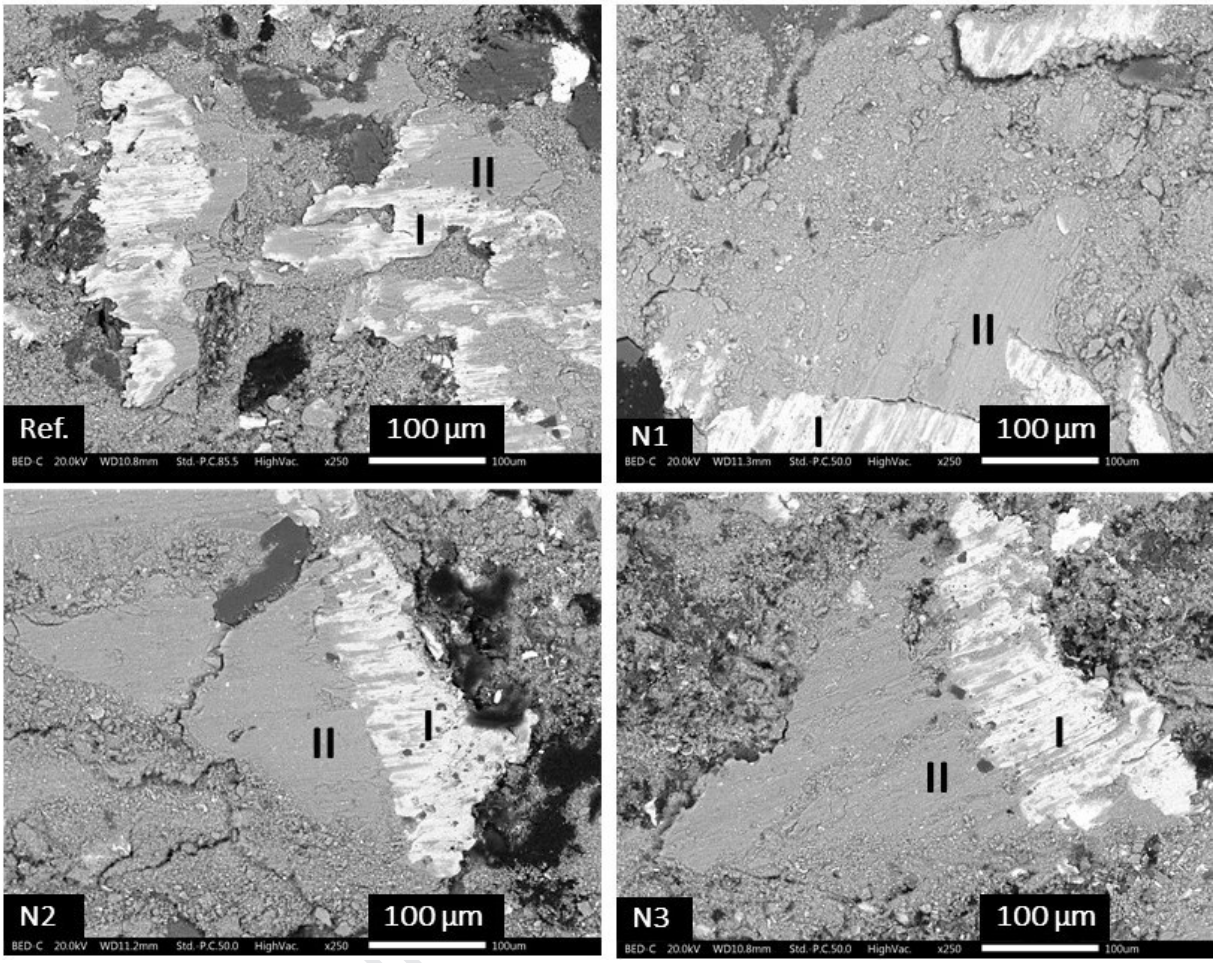

Fig. 11 SEM observations of pins surface after the pin-on-disc tests carried out at *RT_after HT*. Materials: *Ref.*, *N1*, *N2*, *N3*. Primary (I) and secondary (II) plateaus are marked.

Table 8. EDXS analyses on the secondary plateaus of the samples *Ref.*, *N1*, *N2*, *N3* tested at ***RT_after HT***. Concentrations in wt.%.

	Ref.	**N1**	**N2**	**N3**
Fe	63.9	61.6	62.2	61.8
O	17.3	17.7	18.7	18.1
C	6.6	6.8	7.2	7.7
Zn	2.7	2.9	2.5	3.3
Sn	1.8	1.9	2.2	2.1
Mg	1.5	2.4	1.6	1.5
Al	1.9	2.2	1.4	1.6
S	1.5	1.7	1.4	1.5
Si	1.4	1.6	1.4	1.2
Cr	0.6	0.6	0.5	0.5
Ca	0.8	0.6	1.0	0.5

Fig. 12 shows for the four samples the carbon content (wt%) in the secondary plateaus after the tests at *RT_after HT*. The black bars represent the values obtained with the sample tested at *RT_after HT*, while the white bars are for the tests conducted at *RT*. A general decrease in carbon concentration is observed in the secondary plateaus formed after the tests at high temperature (*RT_after HT*). Even in these tests the samples *N2* and *N3* have a higher concentration of carbon (7.2 wt% and 7.7 wt% respectively) compared to the samples *Ref.* and *N1* (6.6 wt% and 6.8 wt% respectively).

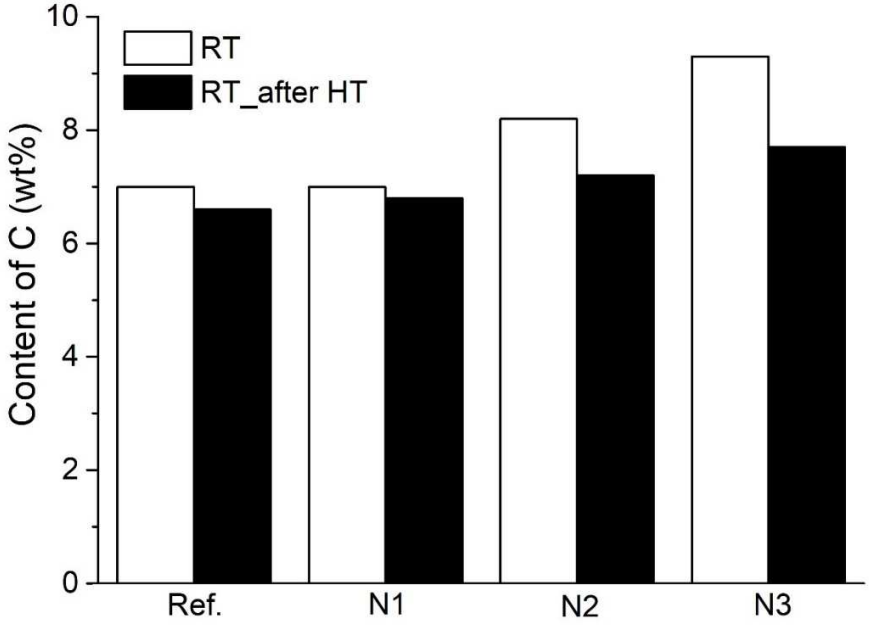

Fig. 12 Content of C (wt%) in the secondary plateaus after the tests at RT_after HT (black bars) compared to the RT tests (white bars).

4. DISCUSSION

In the present work we have investigated the role of graphite as concerns the tribological properties of brake friction materials. Natural graphite reduces the friction coefficient (μ), and, in particular, the friction coefficient decreases with the graphite particle size. The same trend was observed as concerns the wear coefficient (K_a): the samples with a finer graphite (*N2*, *N3*) showed K_a values lower than the reference material (*Ref.*, no graphite) and also of the *N1* sample, featuring larger, plate-like flakes of graphite. The relationship between friction coefficient and wear rate for the tested materials is illustrated in **Fig. 13**. A second order polynomial function is fitting the experimental data adequately. The relevant fitting parameters are listed in **Table 9**.

This trend can be interpreted by considering that the tribological characteristics of the friction materials are influenced by the morphology and chemistry of the friction layer that builds up at the interface between the sliding materials [6][28]. Friction is generated by the adhesive and abrasive interactions

between the pin and the disc. The pin, as well as the disc, are possible sources of carbon. In the pin, many carbonaceous constituents are present, other than the deliberately added graphite, like: phenolic resin, coke, rubber and organic fibers. The presence of a relatively high concentration of graphite on the friction surface may contribute to the formation of a graphite-rich friction layer with dense and well compacted secondary plateaus, leading to a general improvement of the friction performances [29][30].

The graphite with smaller particle size enters the friction layer more easily and becomes more homogeneously distributed. This results in the reduction and stabilization of the friction coefficient. In agreement with this situation, the samples with a finer graphite, *N2* and *N3*, displayed better compacted friction layers (Fig. 8), which, also for their graphite content, are responsible for the reduction in the adhesive interaction between the mating surfaces, resulting in a reduction in the wear rate K_a .

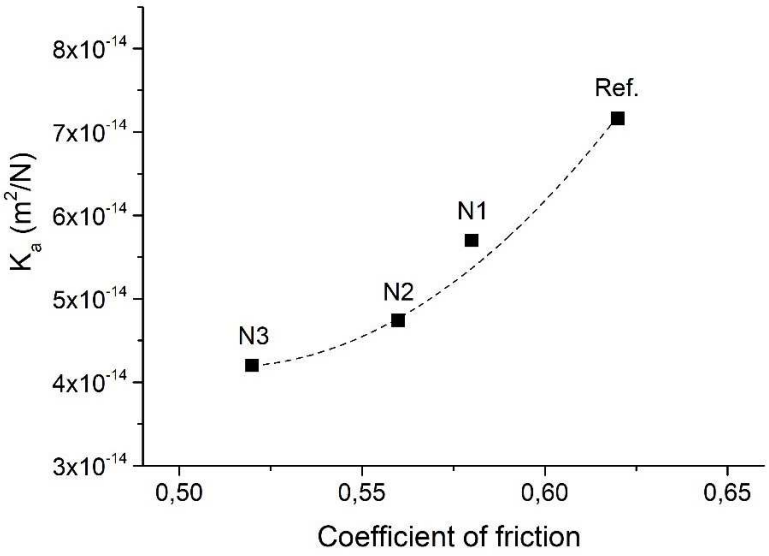

Fig. 13 Relation between the coefficient of friction and the specific wear coefficient (K_a) for the samples: *Ref.*, *N1*, *N2*, *N3*.

Table 9. Parameters of the equation ($y = a + bx + cx^2$) used to fit the data in Fig.12.

a	b	c	Adj. R-Square
$7.27*10^{-13}$	$-2.67*10^{-12}$	$2.60*10^{-12}$	0.98

In **Fig. 14** a schematic representation of the evolution of the friction coefficient curves, typically observed for all the tested materials, under the different test conditions: *RT*, *HT* and *HT_after HT* are shown.

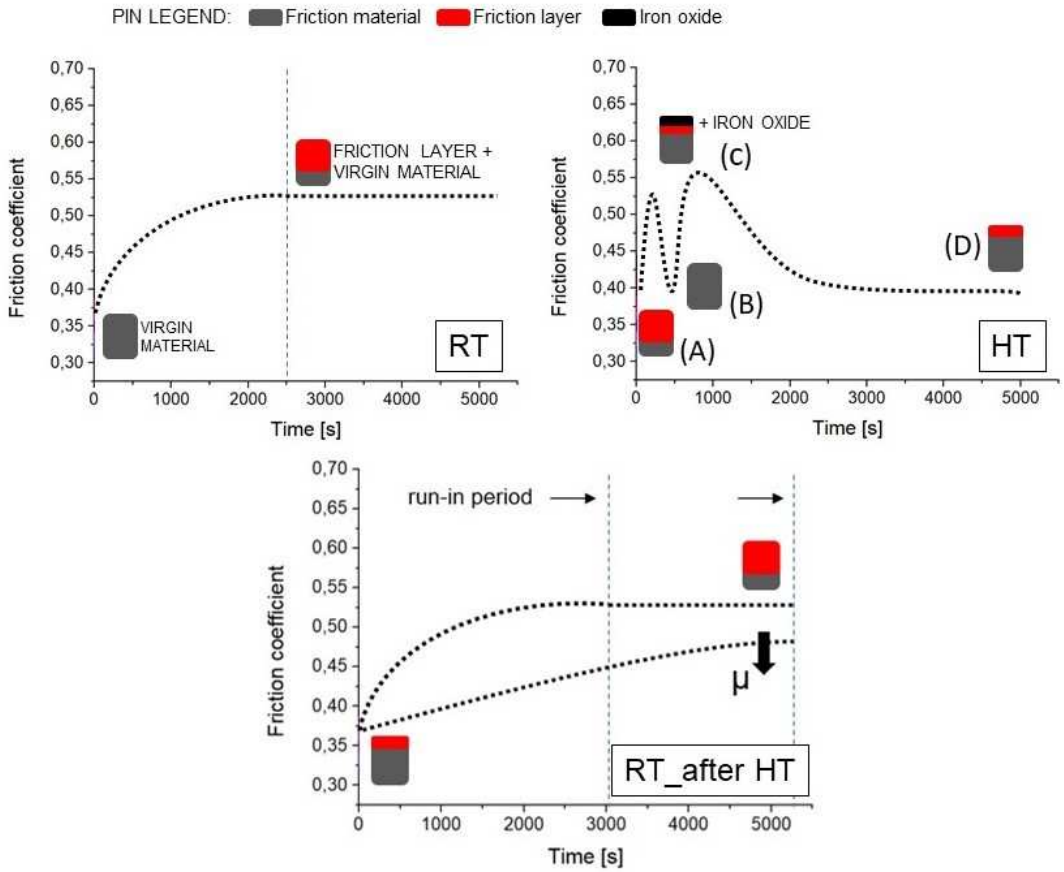

Fig. 14 Schematic representation of the evolution of the friction coefficient for the tests: *RT*, *HT* and *RT_after HT*. The scheme describes the conditions of the surface of the pins during the tests. See the main text for a full description.

In the tests conducted at *RT*, after approximately 2500 s run-in, the coefficient of friction reaches a steady state, determined by the formation of a friction layer, which stabilizes the contact between the pin and the disc.

In the tests at *HT*, the friction coefficient is characterised by a peculiar behaviour, observed in all tests and shown by the relevant (HT) curve in **Fig. 14**. Four main stages can be identified:

(A) A friction layer, which formed during the *RT* test, is already present on the pin's surface at the beginning of the *HT* test. However, since during the heating up, the disc and the pin are not in contact, at the beginning of the test a sort of running-in takes place anyway. It is related to the re-establishment of the full contact between the two mating surfaces.

(B) The friction curve shows a drastic decrease in μ, due to the removal of the friction layer from the pin surface for the combined action of: adhesion forces and thermal softening of the friction material, that is not sustaining any longer the original surface layer. It has to be considered that during the test at 400°C, a thermal degradation of the phenolic resin occurs [31]. As clearly evidenced in a previous investigation [32], this reduces the capability of the underlaying friction

material to sustain the friction layer adequately. Moreover, an abrasion contribution from the oxide forming on the disc surface is certainly contributing to removing the original friction layer from the pin surface.

(C) Disc oxidation and wearing out of the pin surface determine a new raise in the friction coefficient, accompanied by the formation of a new friction layer, made of the debris coming from both mechanisms. A similar behaviour was observed by Vergne et al. [33], studying the high temperature dry sliding of two steels. Specific PoD tests were interrupted after different time intervals in order to define the contribution from the oxides on the evolution of the coefficient of friction, very similar to that displayed in **Fig. 14**.

(D) Once a maximum value of the friction coefficient is achieved, another decrease is observed. The new reduction in the friction coefficient is due to the combined effect of: the friction material softening and its transfer onto the disc surface, as reported already in similar experiments [32]. This determines the progressive transition from a friction material-cast iron coupling towards a situation in which the friction layer on the pin surface is in sliding contact with the transfer layer on the disc. A steady condition is thus achieved, featuring the stabilization of μ at low values. As depicted by **Fig. 10**.

The influence of graphite particle size at high temperatures was evaluated with the *Eq.2*. The decrease in the friction coefficient observed after the *HT* tests ($\%\mu_{HT}$) showed no significant differences among all samples. It can be concluded that graphite does not significantly influence the behaviour at high temperature. Its role of solid lubricant and friction coefficient stabilizer is jeopardized at high temperature by oxidation phenomena, considering that flash temperatures reached at the contacting asperities of the pin-disc mating surfaces may very easily overcome 400°C [34]. Graphite and other constituent are quickly removed as worn debris [35], and indeed all the samples tested at *HT* show a drastic increase in the specific wear coefficient (K_a).

In the tests at RT after the high-temperature tests (**Fig. 14,** *RT_after_HT*) a friction layer, which formed during the *HT* tests, is already present on the pin surface. Since it is discontinuously distributed on the pin surface (**Fig. 10**), a run-in is necessary before reaching the steady state in the new test conditions.

The Eq.3 gives an indication of the recovery attitude of the tribological properties by the different materials after the *HT* tests [36]. Lower values of the friction coefficient with respect to the initial tests at *RT* were detected in all the samples with graphite additions. The best behaviour in terms of friction coefficient recovery, is observed in the *N3* sample, and this is due to the finer size of added graphite, which makes it easier for the particles to enter the friction layer. In this way, graphite together with other constituents of the friction layer, restore surface conditions similar to those attained at the end of the initial *RT* tests. In this recovery process, it should be considered that the organic components of the friction material (pin), more sensitive to temperature, degraded and were partially emitted from the

tribological system as gaseous products. This reduced their contribution to the growth of the friction layer, and in particular, of the secondary plateaus during the *RT_after HT* tests. The reduction of carbon concentration is confirmed by the pin-pointed EDXS analyses, carried out on the secondary plateaus (**Fig. 12**).

The *Ref.* material displayed the higher specific wear coefficient (see **Fig. 7**) and, at the same time, the better friction coefficient recovery. The relevant scenario emerging from these data is that a rapid restoration of the pin's pristine surface is favoured by the faster wearing out of friction layer, initially present on the pin surface and produced by the *HT* tests.

5.CONCLUSIONS and FUTURE PERSPECTIVES

The effect of natural graphite with different particle size was investigated in a Cu-free friction material using a PoD test rig. The study regarded in the first place the tribological behavior and the formation of the friction layers during the tribological tests on these new materials against pearlitic cast iron. The main results can be summarized as follows:

- The particle size of graphite impacts considerably on the friction, wear properties and friction layer formation.
- In the *RT test*, the larger is the particle size, the larger is the friction coefficient and wear rate.
- The best behavior was observed in the N3 sample, with graphite particle size < 40 µm; in this case the friction coefficient is comparable to the one of the N2 sample (graphite grain size < 100 µm), but with an improvement in the wear performances.
- Graphite particle size < 100 µm render the friction layer more compact and the secondary plateaus more stable, since richer in carbon.
- All tested materials exhibit a reduced percentage of recovery of the friction coefficient after *HT tests* (400°C), which is apparently not affected by the additions of graphite.
- The material without graphite (*Ref.*) retains the better friction-recovery (%) behavior; this is ascribed to a faster wear rate, resulting in a fast restoration of the initial pin's surface conditions.

Two further main investigations on natural graphite are planned to complete the picture.

The first will deal with the estimation of an optimal concentration of graphite. The second research theme concerns the way in which graphite (possibly in different concentrations) affects the particulate matter emissions from the friction materials. Nowadays, this is indeed a major issue in the development of novel friction materials.

Eventually, it would be extremely interesting to perform full dynamometer tests in order to understand the role of graphite particle size on NVH performance of the Cu-free formulations.

ACKNOWLEDGEMENTS

The Authors wish to thank Cinzia Menapace for useful discussions in the earliest phases of the research. The Authors would also like to thank the Imerys and AMG companies, for making the graphite powders used in this research available.

The research has received financial support by the EIT-Raw Materials through the EU Project: ECOPADS – Eliminating COpper from brake PADS & recycling – n. 17182.

REFERENCES

[1] Brake friction material - Restrictions on use, substitute Senate Bill 6557, (2010).

[2] M. Kumar, J. Bijwe, Non-asbestos organic (NAO) friction composites: Role of copper; its shape and amount, Wear. 270 (2011) 269–280. https://doi.org/10.1016/j.wear.2010.10.068.

[3] L.Y. Barros, J.C. Poletto, P.D. Neis, N.F. Ferreira, C.H.S. Pereira, Influence of copper on automotive brake performance, Wear. 426–427 (2019) 741–749. https://doi.org/10.1016/j.wear.2019.01.055.

[4] P. Filip, L. Kovarik, M.A. Wright, Automotive Brake Lining Characterization, in: SAE Tech. Pap. Ser., 2010. https://doi.org/10.4271/973024.

[5] D. Chan, G.W. Stachowiak, Review of automotive brake friction materials, Proc. Inst. Mech. Eng. Part D J. Automob. Eng. 218 (2004) 953–966. https://doi.org/10.1243/0954407041856773.

[6] M. Eriksson, F. Bergman, S. Jacobson, On the nature of tribological contact in automotive brakes, Wear. 252 (2002) 26–36. https://doi.org/10.1016/S0043-1648(01)00849-3.

[7] W. Österle, C. Deutsch, T. Gradt, G. Orts-Gil, T. Schneider, A.I. Dmitriev, Tribological screening tests for the selection of raw materials for automotive brake pad formulations, Tribol. Int. 73 (2014) 148–155. https://doi.org/10.1016/j.triboint.2014.01.017.

[8] A.R. Daei, D. Majumdar, P. Filip, Performance of Low-metallic Cu-free Brake Pads with Two Different Graphite Types, in: SAE Tech. Pap. Ser., 2015. https://doi.org/10.4271/2015-01-2677.

[9] R.C. Dante, Handbook of Friction Materials and their Applications, Elsevier, 2016. https://doi.org/10.1016/C2015-0-00634-7.

[10] W. Sterle, C. Prietzel, H. Kloß, A.I.I. Dmitriev, W. Österle, C. Prietzel, H. Kloß, A.I.I. Dmitriev, On the role of copper in brake friction materials, Tribol. Int. 43 (2010) 2317–2326. https://doi.org/10.1016/j.triboint.2010.08.005.

[11] L. Su, F. Gao, X. Han, R. Fu, E. Zhang, Tribological Behavior of Copper–Graphite Powder Third Body on Copper-Based Friction Materials, Tribol. Lett. 60 (2015) 30. https://doi.org/10.1007/s11249-015-0605-3.

[12] Y. Xiao, Z. Zhang, P. Yao, K. Fan, H. Zhou, T. Gong, L. Zhao, M. Deng, Mechanical and tribological behaviors of copper metal matrix composites for brake pads used in high-speed trains, Tribol. Int. 119 (2018) 585–592. https://doi.org/10.1016/j.triboint.2017.11.038.

[13] S.. Moustafa, S.. El-Badry, A.. Sanad, B. Kieback, Friction and wear of copper–graphite composites made with Cu-coated and uncoated graphite powders, Wear. 253 (2002) 699–710. https://doi.org/10.1016/S0043-1648(02)00038-8.

[14] P. Zhang, L. Zhang, D. Wei, P. Wu, J. Cao, C. Shijia, X. Qu, K. Fu, Effect of graphite type on the contact plateaus and friction properties of copper-based friction material for high-speed railway train, Wear. 432–433 (2019) 202927. https://doi.org/10.1016/j.wear.2019.202927.

[15] P. Cai, T. Wang, Q. Wang, Effect of several solid lubricants on the mechanical and tribological properties of phenolic resin-based composites, Polym. Compos. 36 (2015) 2203–2211. https://doi.org/10.1002/pc.23132.

[16] D. Kolluri, A.K. Ghosh, J. Bijwe, Analysis of load-speed sensitivity of friction composites based

on various synthetic graphites, Wear. 266 (2009) 266–274. https://doi.org/10.1016/j.wear.2008.06.023.

[17] R. Gilardi, L. Alzati, M. Thiam, J.-F. Brunel, Y. Desplanques, P. Dufrénoy, S. Sharma, J. Bijwe, Copper Substitution and Noise Reduction in Brake Pads: Graphite Type Selection, Materials (Basel). 5 (2012) 2258–2269. https://doi.org/10.3390/ma5112258.

[18] N. Aranganathan, J. Bijwe, Special grade of graphite in NAO friction materials for possible replacement of copper, Wear. 330–331 (2015) 515–523. https://doi.org/10.1016/j.wear.2014.12.037.

[19] N. Aranganathan, J. Bijwe, Comparative performance evaluation of NAO friction materials containing natural graphite and thermo-graphite, Wear. 358–359 (2016) 17–22. https://doi.org/10.1016/j.wear.2016.03.032.

[20] D.K. Kolluri, X. Boidin, Y. Desplanques, G. Degallaix, A.K. Ghosh, M. Kumar, J. Bijwe, Effect of Natural Graphite Particle size in friction materials on thermal localisation phenomenon during stop-braking, Wear. 268 (2010) 1472–1482. https://doi.org/10.1016/j.wear.2010.02.024.

[21] N. Aranganathan, J. Bijwe, Development of copper-free eco-friendly brake-friction material using novel ingredients, Wear. 352–353 (2016) 79–91. https://doi.org/10.1016/j.wear.2016.01.023.

[22] P. Chandra Verma, L. Menapace, A. Bonfanti, R. Ciudin, S. Gialanella, G. Straffelini, Braking pad-disc system: Wear mechanisms and formation of wear fragments, Wear. 322–323 (2015) 251–258. https://doi.org/10.1016/j.wear.2014.11.019.

[23] C. Menapace, M. Leonardi, V. Matějka, S. Gialanella, G. Straffelini, Dry sliding behavior and friction layer formation in copper-free barite containing friction materials, Wear. 398–399 (2018) 191–200. https://doi.org/10.1016/j.wear.2017.12.008.

[24] G.P. Ostermeyer, M. Müller, Dynamic interaction of friction and surface topography in brake systems, Tribol. Int. 39 (2006) 370–380. https://doi.org/10.1016/j.triboint.2005.04.018.

[25] M. Federici, S. Gialanella, M. Leonardi, G. Perricone, G. Straffelini, A preliminary investigation on the use of the pin-on-disc test to simulate off-brake friction and wear characteristics of friction materials, Wear. 410–411 (2018) 202–209. https://doi.org/10.1016/j.wear.2018.07.011.

[26] M. Alemani, S. Gialanella, G. Straffelini, R. Ciudin, U. Olofsson, G. Perricone, I. Metinoz, Dry sliding of a low steel friction material against cast iron at different loads: Characterization of the friction layer and wear debris, Wear. 376–377 (2017) 1450–1459. https://doi.org/10.1016/j.wear.2017.01.040.

[27] H.J. Noh, H. Jang, Friction instability induced by iron and iron oxides on friction material surface, Wear. 400–401 (2018) 93–99. https://doi.org/10.1016/j.wear.2017.12.025.

[28] M. Leonardi, C. Menapace, V. Matějka, S. Gialanella, G. Straffelini, Pin-on-disc investigation on copper-free friction materials dry sliding against cast iron, Tribol. Int. 119 (2018) 73–81. https://doi.org/10.1016/j.triboint.2017.10.037.

[29] Y. Zhan, G. Zhang, Friction and wear behavior of copper matrix composites reinforced with SiC and graphite particles, Tribol. Lett. 17 (2004) 91–98.

[30] H. Yang, R. Luo, S. Han, M. Li, Effect of the ratio of graphite/pitch coke on the mechanical and tribological properties of copper–carbon composites, Wear. 268 (2010) 1337–1341.

https://doi.org/10.1016/j.wear.2010.02.007.

[31] C. Menapace, M. Leonardi, M. Secchi, A. Bonfanti, S. Gialanella, G. Straffelini, Thermal behavior of a phenolic resin for brake pad manufacturing, J. Therm. Anal. Calorim. 137 (2019) 759–766. https://doi.org/10.1007/s10973-019-08004-2.

[32] P.C. Verma, R. Ciudin, A. Bonfanti, P. Aswath, G. Straffelini, S. Gialanella, Role of the friction layer in the high-temperature pin-on-disc study of a brake material, Wear. 346–347 (2016) 56–65. https://doi.org/10.1016/j.wear.2015.11.004.

[33] C. Vergne, C. Boher, R. Gras, C. Levaillant, Influence of oxides on friction in hot rolling: Experimental investigations and tribological modelling, Wear. 260 (2006) 957–975. https://doi.org/10.1016/j.wear.2005.06.005.

[34] G. Sutter, N. Ranc, Flash temperature measurement during dry friction process at high sliding speed, Wear. 268 (2010) 1237–1242. https://doi.org/10.1016/j.wear.2010.01.019.

[35] S.-X. Xiao, C.-S. Huang, Y.-L. Li, Carbon Materials, in: Mod. Inorg. Synth. Chem., Elsevier, 2017: pp. 429–462. https://doi.org/10.1016/B978-0-444-63591-4.00016-1.

[36] B.K. Satapathy, J. Bijwe, Fade and Recovery Behavior of Non-Asbestos Organic (NAO) Composite Friction Materials based on Combinations of Rock Fibers and Organic Fibers, J. Reinf. Plast. Compos. 24 (2005) 563–577. https://doi.org/10.1177/0731684405043561.

Highlights

- Graphite's granulometry in a copper-free friction material was investigated.
- The new formulations were characterized running pin-on-disc tests.
- Shape and size of the graphite particles influence the tribological properties.
- Fine graphite particle size renders the friction layer more compact and stable.

Declaration of interests

☒ The authors declare that they have no known competing financial interests or personal relationships that could have appeared to influence the work reported in this paper.

☐The authors declare the following financial interests/personal relationships which may be considered as potential competing interests: